The Cloud-Vegetation Interaction in a Future Climate

LES study on the effects of enhanced CO_2 concentrations and a higher temperature on the formation of cumulus clouds

bsnscb.com

Tim Voskamp

The Cloud-Vegetation Interaction in a Future Climate

LES study on the effects of enhanced CO_2 concentrations and a higher temperature on the formation of cumulus clouds

Tim Voskamp

Supervisors:
ir. Martin Sikma
Prof. Dr. Jordi Vilà-Guerau de Arellano

MSc Thesis
Wageningen, July 2017
Meteorology and Air Quality Section
Wageningen University, The Netherlands

Abstract

We studied the cloud-vegetation interaction in a future climate by means of an increase in the atmospheric CO_2 concentration and temperature. Understanding the feedbacks between surface and atmosphere is essential in climate modelling, especially with the eye on the future as those feedbacks are influenced by changes in temperature and CO_2. We used the Dutch Atmospheric Large Eddie Simulation (DALES) model coupled to the plant physiological A-g_s model and executed four numerical simulations (Present, CO2, Temp and Future) where CO_2 and temperature were separately increased with 200 ppm in the CO2 run and 2 Kelvin in the Temp run, and simultaneously in the Future run.

We found that due to an additional supply of CO_2 the assimilation and canopy resistance were increased (physiological forcing of CO_2), resulting in a decrease of the latent heat flux (LE) and a subsequent increase of the sensible heat flux (H). Thermals contained less moisture but had more energy, which resulted in a larger cloud cover and a shifting of the distribution of optical cloud thickness τ (tau) to more thicker and less thinner (forced) clouds. Warming exactly had the opposite effect as LE is enhanced following the Clausius-Clapeyron relation, resulting in a lower H and a subsequent decrease of energy and thermal strength, leading to fewer clouds and a shifting of the tau distribution towards more thinner and less thicker clouds. Both forcings combined resulted in fewer and thinner clouds, despite that thermals contained more energy, indicating that temperature is a stronger forcing than CO_2.

Since we cannot provide a satisfactory explanation for the decrease in cloud cover in the Future run, more detailed research on the processes and feedbacks within the cloud-vegetation system is needed, selecting only above updrafts instead of focussing on domain averages.

Contents

1 Introduction

Although feedbacks between the surface and atmosphere play a key role within climate simulations, it is difficult to correctly represent their underlying mechanisms in a model (Bonan, 1995; Seneviratne et al., 2006). A large uncertainty arises in the modelling of cumulus clouds as these clouds behave chaotically, have a short lifetime (about 7 minutes) (Horn et al., 2015) and are not explicitly resolved since they are a sub-grid phenomenon (Tiedtke et al., 1988; Huang and Margulis, 2013), having a length scale of about 500 meters (Horn et al., 2015). Still, their impact is significant as in the shade of clouds the available energy diminishes, resulting in a decrease of the fluxes of the Surface Energy Balance (SEB) (Sikma et al., 2017). Cumulus clouds also play a role in the often rapid transition from shallow to deep convection, influencing the larger scales as well (Kuang and Bretherton, 2006). In a changing climate where more severe weather and extreme precipitation events are observed (Trenberth, 2011), the understanding of feedbacks between clouds and surface is essential. Moreover, as those feedbacks are influenced by higher temperatures and enhanced atmospheric CO_2 concentrations (Cheruy et al., 2014; Vilà-Guerau de Arellano et al., 2012), and keeping in mind that vegetation responses are in particular sensitive (Vilà-Guerau de Arellano et al., 2014), their relevance is expected only to increase.

To understand the development of cumulus clouds, some fundamental research was conducted by several authors. LeMone and Pennell (1976) found that moisture and momentum fluxes in the sub-cloud layer were responsible for the cloud distribution on the scale of individual cumulus clouds, whereas Chen and Avissar (1994) showed that surface's discontinuities changed the timing and onset of clouds. Studying the role of vegetation, Monteith (1995) showed that vegetation regulates boundary-layer growth and the vapour pressure deficit through the closing and opening of plant's stomata. Also Collins and Avissar (1994) highlighted the role of stomata in the variability of the surface fluxes. In recent years the possibilities for research in the vegetation-atmospheric-cloud interaction have increased due to more advanced computational power and a better understanding of fundamental modelling concepts in relation with the former. The Large Eddy Simulation (LES) technique proved to be a useful tool to interactively study the coupling between vegetation, turbulent transport and clouds in 3D, thereby including the shading effects of clouds (Lohou and Patton, 2014; Horn et al., 2015; Vilà-Guerau de Arellano et al., 2014). Lohou and Patton (2014) showed that the shading effect of shallow cumulus clouds caused a difference in the partitioning between sensible and latent heat at a non-vegetated surface. The response was highly non-linear, having a larger effect on the sensible heat flux compared to the latent heat flux. With other LES experiments, Horn et al. (2015) showed that shading of cumulus clouds resulted in smaller and more clouds, caused by a decrease in the turbulent kinetic energy, which was the result of a local decrease in incoming radiation beneath the cloud, surface heterogeneity dynamics and a smaller convective velocity. Focussing on the role of vegetation, Vilà-Guerau de Arellano et al. (2014) coupled a plant-physiology model to LES and found that shading resulted in a high spatial variability of the surface fluxes. They also showed that above vegetation with C4 plants the cloud cover is larger than above C3 plants, as C4 plants have a larger water use efficiency (WUE) than C3 plants, resulting in a larger surface resistance, a lower latent heat flux and a subsequently larger sensible heat flux. More vigorous and deeper thermals increased the cloud cover, despite that they transported less moisture.

Vilà-Guerau de Arellano et al. (2014) also indicated that the stomatal relaxation time (the stomatal response to external factors, e.g. the passage of a cloud) has consequences for turbulence, which in turn could affect cloud properties. Based on those findings, Sikma et al. (2017) used LES and varied the stomatal relaxation time and the background wind, concluding that with increasing plant relaxation time and background wind the regional averaged surface conditions become more important than local vegetation-cloud coupling. They also showed that for free convective situations, fluctuations in the surface fluxes are largely determined by the horizontal wind speed (U) through the aerodynamic resistance, fuelled by the changes in the severity of up- and downdrafts. Near updraft regions, the surface fluxes together with assimilation appeared to be larger, predominantly

due to a decrease in r_a. Sikma et al. (2017) also confirmed the findings of Pedruzo-Bagazgoitia et al. (2017) that in the shade of clouds with a thin optical depth ($\tau < 8$) assimilation by plants is increased. This happened because for thin clouds the increase in diffuse radiation is larger than the decrease in direct radiation, resulting in more available radiation for photosynthesis and a decrease of the stomatal resistance.

Up to now, LES research mainly focussed on the vegetation-atmosphere interaction at current climate conditions. Still, other models like General Circulation Models (GCM's) have been used to study the impact of enhanced CO_2 concentrations and higher temperatures in a future climate (Cramer et al., 2001; Boucher et al., 2009; Cao et al., 2010; Andrews and Ringer, 2014). Doutriaux-Boucher et al. (2009) discussed that besides from the radiative forcing, CO_2 also has a physiological forcing. Observations show that in a response to higher CO_2 levels (CO_2 fertilization), plants tend to close their stomata (Ainsworth and Long, 2005; Kruijt et al., 2008), consequently leading to a lower evapotranspiration. Andrews and Ringer (2014) showed with the Hadley Centre Global Environmental Model (HadGem) that over land the low-level cloud amount is decreased if CO_2 (1% yr^{-1} for 140 years) and temperature (2.5 K) are increased and that the physiological forcing of CO_2 is the dominant factor herein.

Vilà-Guerau de Arellano et al. (2012) also studied cloud formation in a future climate using a conceptual mixed-layer model coupled to a land-surface model with a mechanistic representation of the vegetation. Temperature and the CO_2 concentration were increased separately to study the effect of both forcings. The physiological forcing of CO_2 had a negative effect on cloud formation as due to a higher sensible heat flux more heat and less moisture was transported into the boundary layer. Warming increased the latent heat flux, thereby increasing the ability of the atmosphere to take up water, resulting in a positive effect on cloud formation. When both forcings (warming and enhanced CO_2) were included simultaneously, the CO_2 effect dominated, resulting in a net effect of suppressed boundary-layer cloud formation. (Vilà-Guerau de Arellano et al., 2012).

As the results of (Andrews and Ringer, 2014) were obtained with a global (large scale) model and the results of Vilà-Guerau de Arellano et al. (2012) with a relatively simple conceptual model, where for both models thermals and turbulent coherent structures are not explicitly resolved, it would be relevant to apply the far more detailed and advanced LES technique in a new study, resolving ninety percent of the turbulence explicitly and having a large three-dimensional (3D) spatial resolution (Heus et al., 2010)). Also secondary effects as the effect of wind speed on cloud shape, the impact of cloud shading on the surface energy balance, the inclusion of surface heterogeneities, the effect of wind shear on cloud tilting and other local effects are then included. Our study will have a comparable set up as the study of Vilà-Guerau de Arellano et al. (2012), investigating the same case, i.e. a typical autumn day in The Netherlands with cumulus clouds (Casso-Torralba et al., 2008), which is already validated against observations (Vilà-Guerau de Arellano et al., 2012). LES is used to perform four numerical simulations in order to answer the following research question:

- **To what extent is the development of cumulus clouds over land affected by an increase in atmospheric CO_2 and temperature in a future climate?**

With two subquestions:

1. Which forcing (enhanced CO_2 or warming) will have the largest impact on cloud formation?
2. How do clouds characteristics change in a future climate?

2 Methodology

This section starts with describing the main characteristics of the LES model used in this study. Then, the research strategy in order to answer the research questions is discussed. Finally, the methodology section ends with formulating some important surface variables to help understanding possible effects of changes in atmospheric CO_2 and temperature on the surface fluxes.

2.1 Model description

The model used in this study is the Dutch Atmospheric Large-Eddy Simulation model (DALES; version 4.1). It is based on a previous version 3.2 which is extensively described by Heus et al. (2010) and by Ouwersloot et al. (2016) who added some extensions. The model runs on a cartesian grid and the Boussinesq approximation is applied to solve the Navier-Stokes equation, neglecting molecular transport terms. For time integration, the third-order Runge-Kutta scheme is used, where the time step decreases with increasing numerical instability. The interactive plant physiological submodel A-g_s (Jacobs and de Bruin, 1997; Ronda et al., 2001) is included in the Land Surface Model (LSM) and the latter is implemented in DALES as a submodel. The LSM solves the fluxes of the SEB and calculates the soil temperature profile for each grid cell. Concerning the formation of cloud water, the 'all or nothing' principle is used, assuming that no saturation occurs if a grid cell contains no liquid water. The two big-leaf approach introduced by Pedruzo-Bagazgoitia et al. (2017) is used to distinguish between direct and diffuse radiation, and in-canopy radiative transfer.

All model settings are equal to the ones described by Sikma et al. (2017). The surface is covered for 90% by well-watered C3 grass, describing a Soil Moisture Index (SMI) of 0.40, indicating that the soil is between wilting point and field capacity (Betts, 2004). This means that the vegetation does not experience water stress, but conditions are not optimal either. All simulations start at 7 UTC (9 local time), simulating 11.67 hours of daylight. The domain is 48 km x 48 km x 5.5 km with grid spacings of 50 m x 50 m x 12 m (x,y,z). Due to this high resolution the model is able to resolve 90% of all the turbulence within in the boundary layer, needing parametrization only for the small scale turbulence. Figure 2.1 shows a vertical cross section of the liquid water to illustrate the capabilities of the model to capture all the high detail and spatial variability.

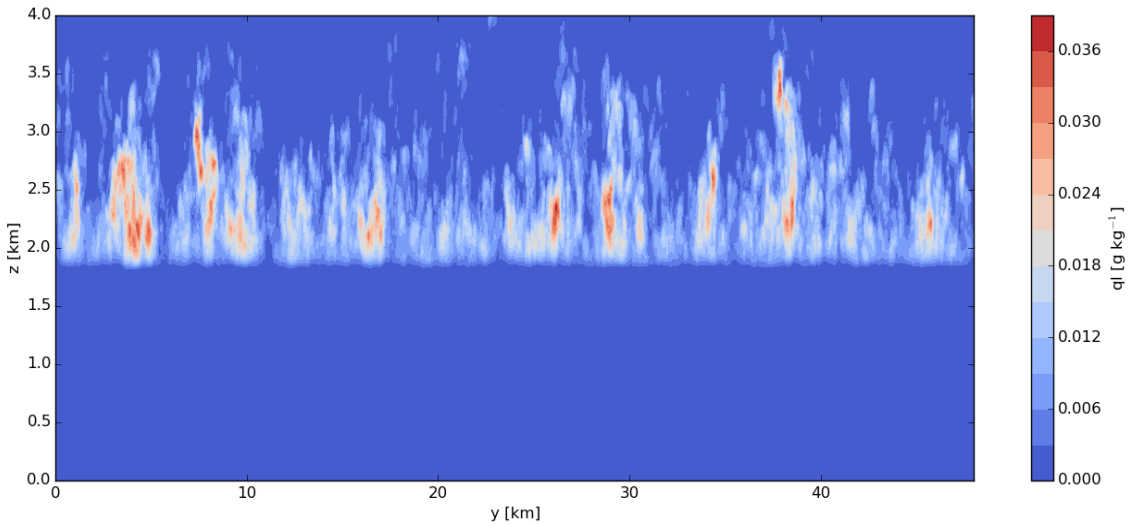

Figure 2.1: Vertical cross-section of the liquid water content at 16 LT, averaged over x. The cloud cover is 19 %.

2.2 Research strategy

The research strategy of this study is equal to Vilà-Guerau de Arellano et al. (2012), so four simulations or runs will be performed. The first one is the control run and is called 'Present'. It represents present climate conditions, indicating an initial atmospheric CO_2 concentration of 418 ppm and an initial temperature of 284 K. This simulation was already available from Sikma et al. (2017). Then, the second run is called 'CO2' and is the same as 'Present', but with the initial atmospheric CO_2 concentration increased from 418 ppm to 618 ppm. The third one is called 'Temp' and is the same as 'Present', but with the initial temperature (soil temperature as well) increased with 2 Kelvin to 286 Kelvin. The IPCC report from 2007 (Solomon, 2007) indicated that the Relative Humidity (RH) is expected to remain equal in the future and this was conformed by Soden and Held (2006). Therefore the initial specific moisture content is increased in order to keep the initial RH equal for every level in de vertical (z) direction. The fourth run is called 'Future' and is a combination of 'CO2' and 'Temp', having both temperature and CO_2 increased. In all runs the background wind is set to 0 m s^{-1}, creating idealized free convective situations. It should be noted that within the model CO_2 only has an effect on the response of the vegetation (physiological forcing). The longwave radiative forcing is excluded, meaning that an increase in CO_2 will not result in an increase in the incoming longwave radiation and affect temperature, making it possible to separately study the impact of both enhanced CO_2 and increased temperatures on the cloud-vegetation interaction. Table 1 gives an overview of the settings of each run together with the color every run will be represented by in the figures in the results section.

Table 2.1: Overview of the initial settings of the Present, CO2, Temp and Future runs and corresponding color.

	Initial CO_2 Concentration [ppm]	**Initial Temperature [K]**	**Color**
Present	418	284	Blue
CO2	618	284	Green
Temp	418	286	Red
Future	618	286	Black

2.3 Formulation of surface variables

In order to explain possible effects of changes in the atmospheric CO_2 concentration and temperature, it is necessary to understand how the surface responds to changes in atmospheric variables like radiation, temperature and humidity. As those changes are expected to influence plant's photosyntheses (Vilà-Guerau de Arellano et al., 2012), first the net assimilation A_n will be considered, which is the gross assimilation minus the dark respiration. A_n is defined as the flux from the atmosphere into the plant and has therefore negative values. At leaf level it is represented by the following equation (Jacobs and de Bruin, 1997):

$$A_n = \frac{c_a - c_i}{r_a + r_{c_{CO_2}}}, \tag{2.1}$$

where c_a and c_i are the CO_2 concentrations outside and inside the leaf, r_a is the aerodynamic resistance and $r_{c_{CO2}}$ is the stomatal resistance for CO_2. The latter indicates that if plants close their stomata, assimilation is decreased by means of a increase in the stomatal resistance. The pathway through the stomata for CO_2 and water is the same, but due to a difference in the molecular diffusion their stomatal resistance can be related to $\frac{r_{c_{H_2O}}}{r_{c_{CO_2}}} = 1.6$ (Jacobs and de Bruin, 1997). The aerodynamic resistance indicates how easily the exchange of heat and water vapour proceeds and is dependent on the horizontal wind speed (U) and the surface drag coefficient (C). Note that the soil respiration is not included in the net assimilation.

Next to the net assimilation, the fluxes of the surface energy balance also play a key role in the surface-atmosphere coupling. The SEB is defined as follows (Jacobs and de Bruin, 1997):

$$Q_{net} = LE + H + G, \tag{2.2}$$

where Q_{net} is the net radiation, LE is the latent heat flux, H is the sensible heat flux and G is the soil heat flux. The LE, H and G fluxes divide the available available energy from the net radiation. The latent heat flux uses the energy to evaporate water and is defined as (Jacobs and de Bruin, 1997):

$$LE = \frac{\rho L_v}{r_a + r_{c_{H_2O}}} (q_s(T_c) - q), \tag{2.3}$$

where ρ is the surface air density, L_v is the latent heat constant for evaporation, q and q_s represent the actual and saturated specific moisture content or humidity just above the vegetation, where the latter is dependent on the canopy temperature (T_c). The difference between the saturated and actual specific moisture content is also known as the water vapour pressure deficit (VPD), as the specific moisture content or specific humidity is directly related to the vapour pressure of water e. Since the latent heat flux is dependent on $\mathrm{r}_{c_{H_2O}}$, it is dependent on $\mathrm{r}_{c_{CO_2}}$ as well. In the results, we scale up the analysis from leaf to canopy, using a canopy resistance r_c instead of a stomatal resistance. Since our main interest lies in the water balance (clouds consist of water), this canopy resistance is based on the stomatal resistance of water, $\mathrm{r}_{c_{H_2O}}$.

Where the latent heat flux uses energy to evaporate water, the sensible heat flux uses energy to heat up the atmosphere. It is defined as (Jacobs and de Bruin, 1997):

$$H = \frac{\rho c_p}{r_a} (\theta_c - \theta), \tag{2.4}$$

where c_p denotes the specific heat of air at constant pressure and θ_c and θ are the canopy and near-surface air potential temperature.

Finally the soil heat flux uses energy to heat up the soil and is defined as:

$$G = \Lambda(\theta_c - \theta_{soil}), \tag{2.5}$$

where Λ is the soil conductivity and θ_{soil} is the temperature of the first soil layer.

3 Case description

In order to get a good understanding of the atmospheric structure on a general day with cumulus clouds, the case is extensively discussed, showing the evolution and vertical profiles of some key variables. We base the analysis of the case on the control run, 'Present', defined in section 2.2. This also indicates that the figures in this section are not observations, but obtained by the model.

The case represents a convective day on 25 September 2003 in Cabauw, The Netherlands. The synoptical situation was anticyclonic with South Easterly winds and large scale advection of heat and CO_2 was negligible (Casso-Torralba et al., 2008). Initially no clouds arose on that day, but since the agreement between the model and observations was strong, that day still was chosen. The soil moisture was decreased in order to increase the sensible heat flux, enhancing cloud formation (Vilà-Guerau de Arellano et al., 2014). With this adjustment, the case represents the development of a typical diurnal atmospheric boundary layer, where thermals originating from the surface underlay the formation of cumulus clouds, reaching a maximum cloud cover of around 20%. As aforementioned, for this case the model is already validated against observations which were collected from the 213-meter tower in Cabauw (Vilà-Guerau de Arellano et al., 2012). Table A2 and A3 of the paper of Vilà-Guerau de Arellano et al. (2014) show the initial and boundary conditions prescribed for this control case. Only the wind (0 m s^{-1} in our study) and numerical settings are different as the latter were equal to the settings of Sikma et al. (2017) as explained in section 2.1.

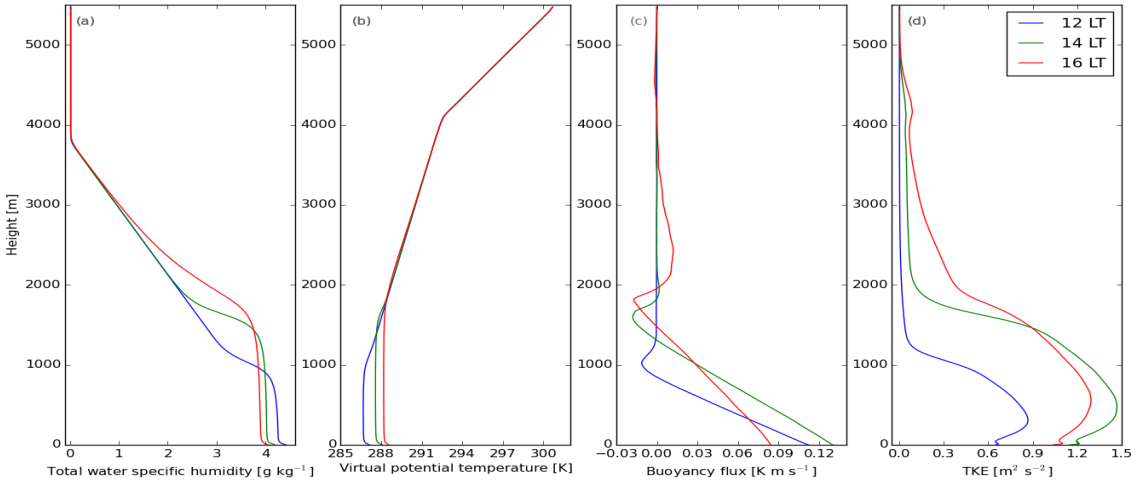

Figure 3.1: Vertical profiles of the total water specific humidity (a), virtual potential temperature (b), buoyancy flux (c) and turbulent kinetic energy (d) at 12:00 LT (0 % cloud cover), 14:00 LT (9 % cloud cover) and 16:00 LT (19 % cloud cover), domain averaged.

On the basis of the vertical profiles of the total water specific humidity (qt), the virtual potential temperature (θv), the buoyancy flux and the Turbulent Kinetic Energy (TKE) for three different times of the day already a good case characterization can be made, where the TKE represents a measure for the amount of turbulence. The three chosen times include a time with no cloud cover (at 12:00 LT), a time with beginning clouds (9% cloud cover at 14:00 LT) and a time with maximum cloud cover (19% at 16:00 LT). Together with the vertical profiles we also analyse the diurnal development of the boundary layer, cloud cover, cloud base and cloud top in figure 2.3.

The case follows a typical convective boundary layer as we can distinguish the different regions of the CBL, focussing on the vertical profiles of qt and θv at 12:00 LT in figure 3.1a and 3.1b. The first region, the surface layer, is roughly the lowest 10 % of the CBL and is characterized by thermally unstable stratified conditions during daytime, explaining the decrease in θv and qt with

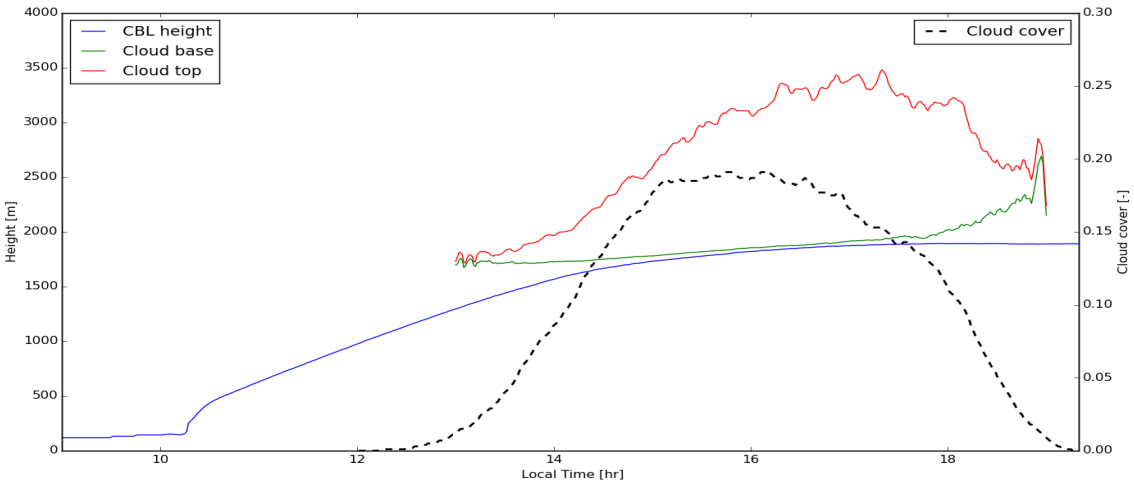

Figure 3.2: Diurnal variation of the boundary layer height, cloud base and cloud top on the left y-axis and the diurnal variation of the cloud cover on the right x-axis, all domain averaged.

height for the first 100 meters (Gentine et al., 2013). The layer is driven by the sensible and latent heat flux that generate turbulent eddies, transporting moisture and heat from the surface into the well-mixed layer above. Within the well-mixed layer, the eddies grow towards stronger and more vigorous thermals, leading to strong turbulent mixing throughout the whole layer, explaining the increase in TKE at around 100 meters. Due to this mixing, q and θv are constant with height, until the begin of the inversion layer at around 1000 meters.

The inversion layer is characterized by stable stratified conditions, i.e. an increase of θv with height. It is the connection between the well-mixed layer below and the warmer and drier atmosphere above, known as the Free Troposphere (FT). Due to this inversion, the buoyancy flux (figure 3.1c) becomes negative at 800 meters as warmer and drier air is entrained from the free troposphere into the mixed layer. This negative buoyancy prevents air parcels to rise any further as they become colder than their environment and sink back. Only thermals with enough energy and positive vertical velocity (updrafts) can overcome the negative buoyancy and penetrate the inversion layer (overshooting thermals), exchanging heat and moisture with the FT. Note that around 4100 meters, there is another stronger inversion, known as the absolute inversion. This absolute inversion is the reason that there is only shallow convection, but we will elaborate on that later.

During the day the sun provides more and more energy to heat up the surface, increasing temperature and density fluctuations, leading to a larger buoyancy flux and TKE at 14:00 LT and 16:00 LT. This results in stronger thermals, increasing the amount of thermals capable of penetrating the inversion layer which results in a shifting of the inversion layer towards a higher level. This explains why at 14:00 LT and 16:00 LT, qt and θv are constant for a larger height compared to 12:00 LT and why the CBL height in figure 3.2 increases during the day. The CBL height in figure 3.2 is defined as the lowest height where the gradient of the potential temperature exceeds 50% of the maximum gradient (Vilà-Guerau de Arellano et al., 2014).

At 14:00 LT and 16:00 LT we also start to find the evidence for the presence of clouds. In figure 3.1a, the transition between the CBL and the FT around 1000 meters is quite abrupt, whereas at 16:00 LT this transition, now around 1700 meters, is smoother, indicating the presence of liquid water. Within the model, the cloud base or Lifting Condensation Level (LCL) is defined as the lowest height where the liquid water content is larger than 0.0025 g kg^{-1}. Figure 2.3 shows that around 12:30 LT the first clouds start to arise, eventually developing towards a height of around

3500 meters till around 19:00 LT the clouds disappear again. We define the cloud layer as the difference between the LCL and the cloud top, and the well-mixed layer below the cloud layer is called the subcloud layer.

Figure 2.3 also shows that the cloud base is always above the CBL. This means that only thermals with enough positive vertical velocity and energy to overcome the negative buoyancy can be lifted and cooled enough to become saturated. Whether or not a thermal becomes an active cloud not only depends on the probability of reaching the LCL, but also on reaching the Level of Free Convection (LFC). The LFC is defined as the height where the buoyancy flux above the subcloud layer become positive again (Crook, 1996). If a thermal has enough energy to reach the LCL, but not enough energy to reach the LFC, a forced cloud will arise (Stull, 1985). This means that the thermal cannot overcome all the negatively buoyant energy and that the cloud will disappear. The amount of negative buoyant energy is defined as the Convective Inhibition (CIN) (Colby Jr, 1984). In order to clarify these concepts a bit more, in figure 2.4 a conceptual picture is shown with the CBL height, LCL and LFC indicated. The figure is based on a vertical profile of the buoyancy flux. In this example, the CIN is all the negative buoyancy integrated from the level where the buoyancy becomes zero at 1500 to the LFC at 1950 meters.

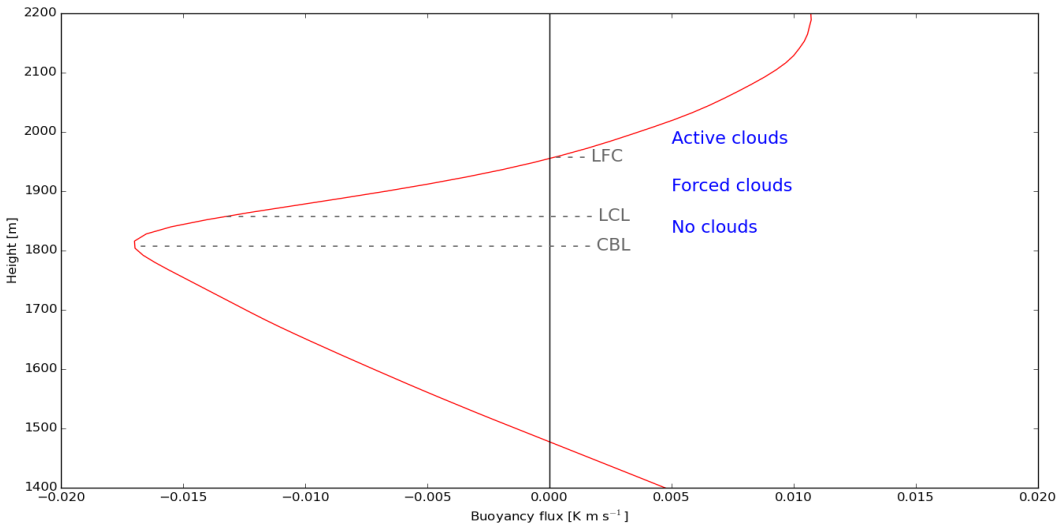

Figure 3.3: Conceptual picture of the height of the CBL, LCL and LFC, using a vertical profile of the buoyancy flux, zoomed in to upper part of the boundary layer and just above.

If a thermal does have the energy to overcome the CIN and reach the LFC, it can grow towards an active cloud as it becomes positively buoyant again due to the release of latent heat, following the moist adiabatic lapse rate within the cloud layer. However, figure 2.2c shows that this situation with positive buoyancy stops around 3700 meter. If we then go back to figure 2.2b, the absolute inversion is located at 4100 meters. Air parcels stop rising as the release of latent heat is not enough for an air parcel to be warmer than it's environment, going from a conditionally unstable situation to an absolute stable situation. This explains why the absolute inversion causes the convection to be only shallow, preventing thunderstorms and deep convection to occur. The level where air parcels lose their positive buoyancy and cannot grow further is called the Level of Neutral Buoyancy (LNB)(Mapes, 2000). The positive buoyant energy integrated from the LFC to the LNB is called the Convective Available Potential Energy (CAPE). If the CIN is small and the CAPE is large, this is a positive indication for the triggering of convection and clouds (Mapes, 2000).

4 Results

We start this section by describing the effects of enhanced CO_2 concentrations, higher temperatures and the combined effect on the vegetation, surface fluxes and atmospheric structure. This is followed by describing the effects of the same forcings, but then focussing on the consequences for clouds. By doing so, we build up the analysis from low to high (surface - atmosphere - clouds).

4.1 Structures of the surface and atmosphere in a future climate

We first consider the effect of increasing the CO_2 concentration with 200 ppm, comparing the CO2 run with the Present run. Then the effect of an increase in temperature with 2 Kelvin is analysed, ending this section with the combined effect of both forcings.

4.1.1 Effects of enhanced CO_2

We start our analysis by focussing on the net assimilation A_n. Assimilation is dependent on the photosynthetically active radiation (PAR), canopy temperature T_c and internal CO_2 concentration c_i (Jacobs, 1994). In figure 4.1a the diurnal variation of A_n is plotted, where the highest values are found at 14:00 LT when the power of the sun is maximal. Willmer and Fricker (1996) indicated that the internal CO_2 concentration is a compromise between supplying building material to photosynthesis and keeping a high influx from the atmosphere. In the A-g_s model c_i is mainly dependent on the external CO_2 concentration c_a and the ratio of c_a and c_i (Ronda et al., 2001) (the effect of the CO_2 compensating point is found to be minimal). We find that with a higher external CO_2 concentration (200 ppm increase), c_a/c_i is hardly affected (0.69 for the CO2 run and 0.68 for the Present run averaged over 15:30 - 16:00 LT), which is in accordance with the work of Leuning (1995), who found that c_a/c_i is rather constant . This indicates that an increase in c_a also results in an increase of c_i, from which the latter is found to be 277 ppm, averaged over 15:30 - 16:00 LT. This means that the absolute difference between c_i and c_a increases. If we then link back to equation 2.1 in section 2 this indicates that the net assimilation is enhanced, which is also what we observe in figure 4.1a. The CO2 run has a value of A_n which is $\sim 25\%$ higher than the Present run, averaged over 15:30 - 16:00 LT. In the rest of this study we will always choose the same period of 15:30 - 16:00 to quantify differences between runs, because cloud cover is almost constant on time then, considering it the most relevant timespan of the day.

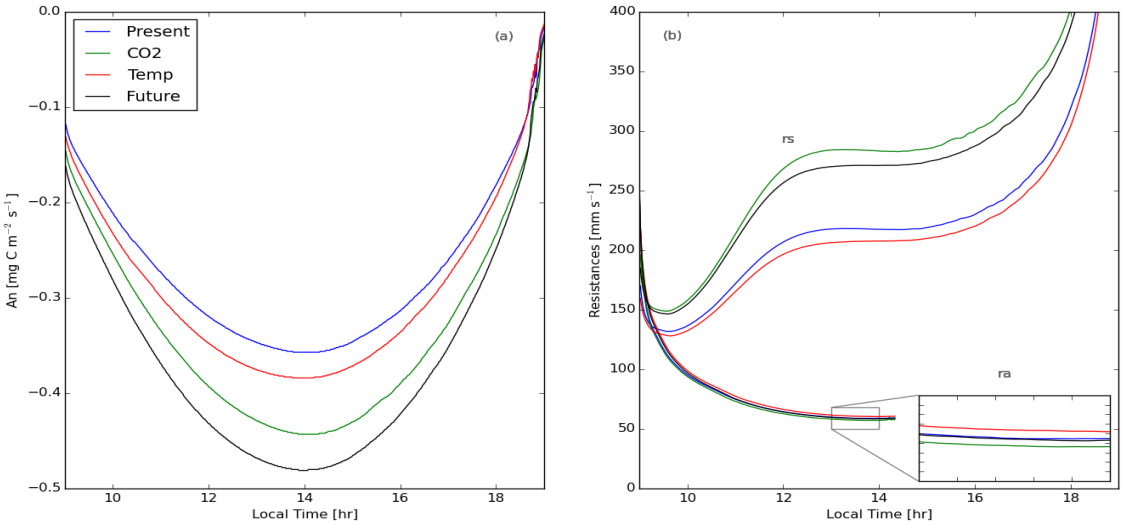

Figure 4.1: Diurnal variation of the net assimilation A_n (a) and canopy r_c and aerodynamic resistance r_a (b) for the Present (blue), CO2 (green), Temp (red) and Future (black) runs, domain averaged.

After assimilation we now focus on the effects of elevated CO_2 on the canopy resistance. The closing and opening of stomata is regulated by means of the turgor pressure in guard cells (Assmann, 1993). Wong et al. (1985) indicated that c_i is hardly affected by assimilation. This indicates that if a larger CO_2 supply is needed, stomata are opened accordingly, whereas with a higher external CO_2 concentration stomata close. The internal CO_2 concentration plays a key role here as due to a higher c_i the membrane potential of guard cells depolarizes by changing ion and solute concentrations, leading to a reduced stomatal aperture (Assmann, 1993). These molecular, biochemical and physiological processes are more extensively described by Ainsworth and Rogers (2007). There is also observational evidence for the increase of r_c as Ainsworth and Long (2005) found a decrease in the stomatal aperture obtained by free-air CO_2 enrichment (FACE) experiments. In the A-g_s model the canopy resistance is directly dependent on the external CO_2 concentration (Ronda et al., 2001), explaining the increase of the canopy resistance with $\sim 30\%$ (again averaged over 15:30 - 16:00 LT), shown in figure 4.1b. Figure 4.1b also shows that there is a minor decrease of the aerodynamic resistance, but this will hardly affect the surface fluxes. The reason for the decrease in r_a will be explained later in this section.

We now turn our attention to the consequences for the surface fluxes. The increased canopy resistances causes the latent heat flux to decrease with $\sim 14\%$ [16 W m^{-2}], which is in accordance with equation 2.3 and shown in figure 4.2. The differences in the available net radiation and soil heat flux are relatively small, i.e. a decrease of $\sim 2\%$ [4 W m^{-2}] for Q_{net} and an increase of $\sim 5\%$ [1 W m^{-2}] for G. This means that the remaining energy, 11 W m^{-2}, is used by the sensible heat flux (an increase of $\sim 10\%$) to heat up the atmosphere, showing that LE and H are always competing for energy as a decrease in LE consequently leads to an increase in H and vice versa.

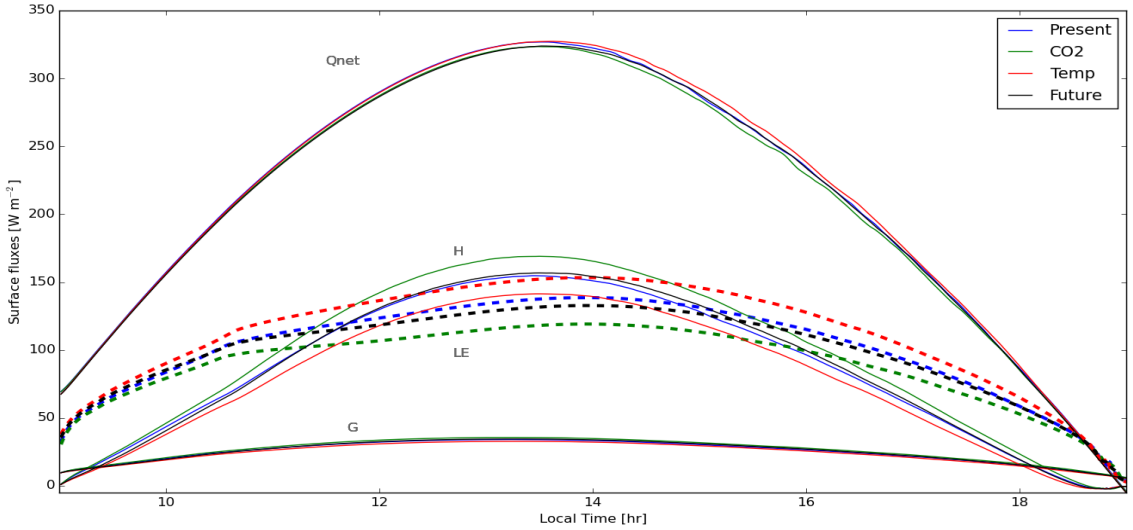

Figure 4.2: Diurnal variation of the net radiation (Qnet), sensible heat flux (H), latent heat flux (LE, dashed) and soil heat flux (G).

The consequences for the buoyancy flux and TKE due to the shift in partitioning of the available energy are plotted in figure 4.3, whereas the consequences for the temperature and humidity are plotted in figure 4.4. Instead of showing three different times, a half hourly average (15:30 - 16:00 LT) is chosen. Due to the increase in the sensible heat flux the atmosphere heats up, increasing the surface buoyancy flux, shown in figure 4.3a and table 4.1. This increases the generation of turbulence as can be derived from figure 4.3b. Since there is more energy in the boundary layer, thermals originating from the surface are stronger, which is also visible in the increase of the convective velocity scale w_*, indicated in table 4.1. The convective velocity scale is the typical velocity of thermals, i.e. a measure for the strength of the thermals, as described by Deardorff (1970) and Holtslag and Moeng (1991). These stronger thermals can penetrate the inversion at a

higher rate than in the Present run, thereby increasing the exchange between the free troposphere and the mixed layer. This in turn enhances the entrainment flux, shown in table 4.1 and figure 4.3a, where the entrainment flux is defined as the most negative value of the buoyancy flux, which is located close to the CBL height at around 1900 meters (Van Stratum et al., 2014). Since both the surface buoyancy flux and the entrainment flux increase, the ratio of both fluxes remains more or less constant, i.e. 0.205 for the CO2 run and 0.202 for the Present run. Based on observations and LES results this ratio is often assumed constant on a value of 0.2 (Tennekes, 1973), meaning that 20 % of the heat contributing to the dynamics of the CBL, originates from the free troposphere.

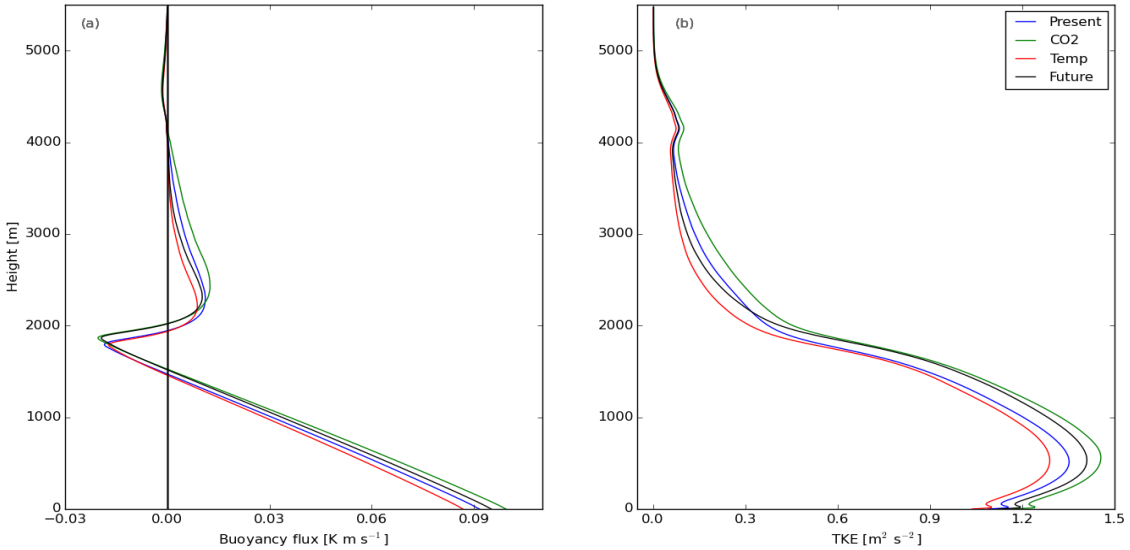

Figure 4.3: Vertical profiles of the buoyancy flux (a) and the turbulent kinetic energy (b), averaged over time from 15:30 - 16:00 LT.

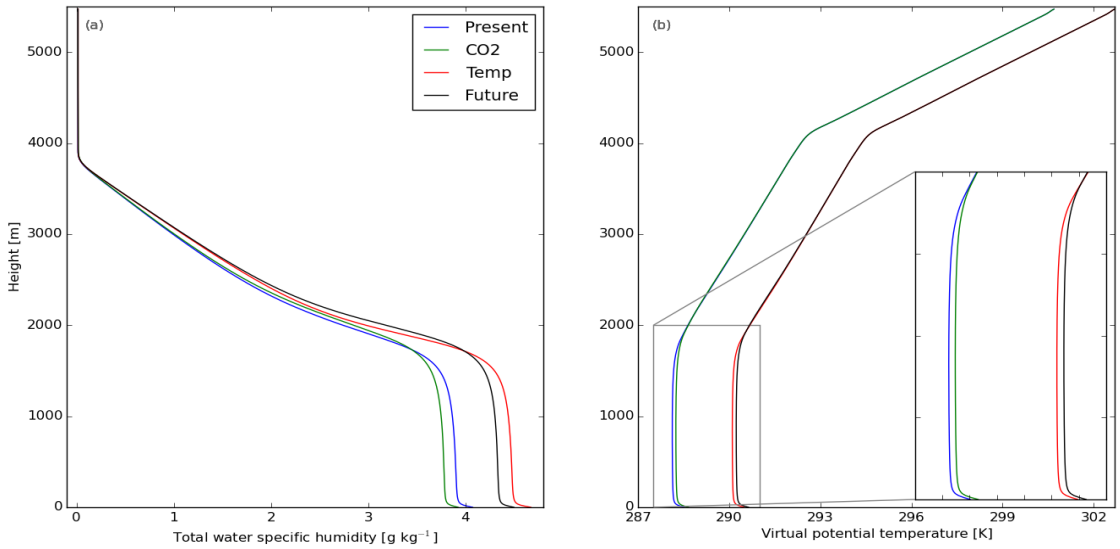

Figure 4.4: Vertical profiles of the total water specific humidity (a) and the virtual potential temperature (b), averaged over time from 15:30 - 16:00 LT.

The higher sensible heat flux in combination with the higher entrainment flux leads to more heat and energy for the boundary layer to grow, leading to a deepening of the CBL, shown in table 4.1. A deeper boundary layer has an diluting effect on the amount of moisture within the CBL, whereas also enhanced dry air entrainment causes the CBL dry out (Van Heerwaarden et al., 2009). In combination with a decreasing latent heat flux, i.e. less water vapour enters the atmosphere, this explains why the total water specific humidity for the CO2 run decreases and why the relative humidity at the surface decreases, shown in figure 4.4a and table 4.1. Since the main alteration originates from the surface (a decrease in H), and since the exchange with the FT is limited, we mainly observe differences in q_t within the boundary layer only. This explains why the value of RH at the top of the CBL is only marginally lower (1%, table 4.1).

Figure 4.4b shows that the boundary layer is not only drier, but warmer as well. Again differences are mainly visible within the CBL (for the same reasons as for q_t). A higher sensible heat flux and more entrainment of warm air causes θ_v to increase, although the heat is divided over a larger area, i.e. the diluting effect of a deeper boundary layer. This also explains why the soil heat flux increases as the canopy temperature is also higher, resulting in an increase of the gradient with the soil temperature in equation 2.5, explaining the increase of G.

Sikma et al. (2017) showed that the surface fluxes are enhanced near rising thermals (updrafts). Below an updraft, air transported upwards has to be supplemented from the sides. This increases the horizontal wind speed U and subsequently decreases the aerodynamic resistance near updraft regions, explaining the increase in the surface fluxes there (Sikma et al., 2017). Figure 4.1 showed that r_a decreases if CO_2 is enhanced. We found that more CO_2 increases the TKE (figure 4.1b), resulting in stronger thermals (higher w_*). This indicates that more air should be supplemented from the sides, resulting in a larger U and a lower r_a. Since we did not quantify differences in U near updraft regions, we present this only as a possible explanation for the increase in r_a. The r_a is only plotted till the moment the larger clouds started to form, as values of r_a started to increase dramatically then. r_a is dependent on the wind speed and the drag coefficient, where the latter tells something about the atmospheric stability. Below a cloud, and with no background wind, almost stable conditions are reached, explaining the very high values for r_a.

As values of the entrainment flux are higher, there is more negative energy that has to be overcome in order to form a cloud. This leads to higher CIN values, shown in table 4.1. On the other hand, CAPE values are also higher (table 4.1) as the CO2 run becomes more positively buoyant than de Present run within the cloud layer at the height of 2100 - 4000 meters. The CIN values are determined by the sum of the buoyancy fluxes at the levels where buoyancy is negative. The CAPE values are determined by the sum of the positive buoyancy fluxes, starting at the level of free convection and ending at the level of neutral buoyancy, as described in section 3.

Table 4.1: Values for the CBL height, relative humidity at the surface and CBL_{top}, convective velocity scale, surface buoyancy flux, entrainment flux, CAPE and CIN, for all runs, averaged over time from 15:30 - 16:00 LT and domain averaged.

	CBL height (m)	**RH surface (-)**	**RH CBL (-)**	**Convective velocity (m s^{-1})**	**Surface Buoyancy flux (K m s^{-1})**	**Entrainment flux (K m s^{-1})**	**CIN (W m^{-2})**	**CAPE (W m^{-2})**
Present	1800	0.40	0.87	1.78	0.092	-0.018	-546	6576
CO2	1873	0.38	0.86	1.85	0.099	-0.020	-623	7406
Temp	1780	0.40	0.87	1.73	0.087	-0.017	-502	6162
Future	1859	0.38	0.86	1.81	0.095	-0.019	-585	7013

4.1.2 Effects of warming

Focussing on the comparison between the Temp run and the Present run in figure 4.1a, we find that the net assimilation is increased when temperature is increased. Plants have an optimum temperature where photosynthesis and assimilation are maximal (Niu et al., 2008). For C3 grass this optimum lies around 298 Kelvin (Jacobs, 1994). For our case, this temperature is not reached, meaning that if we increase the initial temperature to 286 Kelvin we remain left of the optimum, explaining why the net assimilation increases with $\sim 7\%$. Warming not only increases assimilation, but it has an direct effect on the stomatal resistance as well (Willmer and Fricker, 1996). With a higher temperature the metabolism of the guard cells is increased, resulting in an opening of the stomata (Willmer and Fricker, 1996). In the A-g_s model, the temperature effect is visible in the mesophyill conductance, gross assimilation and vapour pressure deficit, which all affect the canopy conductance (Ronda et al., 2001). Figure 4.1b shows that warming eventually leads to a decrease of the canopy resistance with $\sim 4\%$.

Moving back to figure 4.2 again, the latent heat flux has increased with $\sim 11\%$ [13 W m^{-2}] compared to the Present run. To explain this, equation 2.3 is considered. The saturated vapour pressure or specific moisture content q_s follows the Clausius-Clapeyron relation, i.e. warmer air contains more water and therefore q_s increases. The actual vapour pressure also increases in order to have an equal initial relative humidity for the Temp and Present run, as discussed in section 2.2. However, the Clausius-Clapeyron relation is exponential, so q_s increases at a faster rate than q, thereby increasing the vapour pressure deficit for the Temp run. Together with the slight decrease in the canopy resistance this explains why LE increases. As more energy is used to evaporate water, the sensible heat flux decreases with $\sim 7\%$ [8 W m^{-2}]. Q_{net} increases with 2 % [5 W m^{-2}] and G decreases with $\sim 3\%$ [1 W m^{-2}] due to the decrease of the gradient between T_c and T_{soil}. From these changes in the surface fluxes, we can conclude that the shift in partitioning of available energy due to warming is opposite compared to enhancing CO_2, which is in accordance with the study of Vilà-Guerau de Arellano et al. (2012).

Due to the opposite shift in the partitioning of available energy the consequences for the amount of buoyancy and TKE are also opposite compared to the CO2 run, shown in figure 4.3. A lower sensible heat flux means lower values for the buoyancy flux, CBL height and the TKE, resulting in a lower entrainment flux and a lower value for w_* (weaker thermals), shown in table 4.1. Due to the decrease in entrainment the CIN is also lower compared to the Present run, but there are also less thermals that are able to reach the LFC and become positively buoyant, resulting in a decrease of the CAPE as well, all shown in table 4.1. The decrease in the convective velocity scale also results in a slightly higher aerodynamic resistance, shown in figure 4.1b, as up- and downdrafts are weaker, expecting to decrease the horizontal wind speed near updraft regions.

Concerning the profiles of temperature and humidity in figure 4.4, it is difficult to distinguish the effects of the change in the surface fluxes as the initial values of θ_v and q_t have increased, shifting the profiles to the right. As a result of this shifting, we can conclude that the boundary layer is warmer and contains more water. Still, table 4.1 shows that both the relative humidity at the surface and the CBL_{top} do not change.

4.1.3 Combined effects of enhanced CO_2 and warming

Again we start our analysis based on the net assimilation, now focussing on the comparison between the Future and the Present run in figure 4.1a. Since both enhanced CO_2 and warming had a positive effect on photosynthesis and assimilation, A_n increases with $\sim 35\%$. Concerning the canopy resistance, warming slightly offsets the increase in r_c due to enhanced CO_2, leading to a net increase of $\sim 25\%$ in the future, shown in figure 4.1b.

Similar to the canopy resistance, warming and enhanced CO_2 have a compensating effect on the SEB as well, shown in figure 4.2. In section 4.1.1 we found that enhanced CO_2 increases the

sensible heat flux and decreases the latent heat flux, whereas in section 4.1.2 we found that this is opposite for warming. Focussing on the combined effect in the Future run, the effect of enhanced CO_2 is slightly stronger as H increases with $\sim 3\%$ [4 W m^{-2}] and LE decreases with $\sim 3\%$ [4 W m^{-2}]. Again, the difference between T_c and T_{soil} has increased due to the increase in H, explaining the increase in the soil heat flux of $\sim 2\%$ [1 W m^{-2}]. The difference in the net radiation is zero.

The increase in the sensible heat flux, together with the increase of the initial temperature with 2 Kelvin causes the Future run to be warmest of all, shown in figure 4.4b. The decrease in the latent heat flux leads to a drier boundary layer compared to Temp, but there is still more moisture in the atmosphere compared to Present due to the initial increase in q, shown in figure 4.4a. The increased sensible heat flux also leads to a higher surface buoyancy flux and generation of turbulence within the boundary layer, shown in table 4.1 and figure 4.3. This also leads to a deeper boundary layer, a higher w_* and a larger entrainment flux compared to the Present run, shown in table 4.1. The compensating temperature effect holds also for these variables as their values may be higher than the Present run, but compared to the CO2 run, their values are lower (table 4.1). Note that above the CBL, from around 2100 meters till the level of neutral buoyancy at around 4000, values for the buoyancy flux and TKE are actually smaller, explaining why the CAPE values in table 4.1 are lower than Present, whereas the CIN values are still larger. In section 4.2 we will elaborate more on this.

Summarizing section 4.1, concerning the surface and the atmospheric structure, the enhanced CO_2 effect is slightly stronger than the effect of warming, resulting in a small increase of H and a small decrease in LE, leading to a warmer future boundary layer containing more moisture, buoyancy and energy. The next section describes how the properties of this future boundary layer affect cloud characteristics.

4.2 Clouds characteristics in a future climate

This section discusses the differences in cloud characteristics between the four simulations. Again, we start our analysis from the perspective of the CO2 run, followed by the Temp run and Future run, comparing all with the Present run.

4.2.1 Effects of enhanced CO_2

The main cloud characteristics studied here are the cloud cover and tau (τ), where the latter is a measure for the cloud thickness, as described by Stephens (1984). Tau depends on the liquid water path, water density and effective droplet radius r_e. We use a r_e of $10\mu m$, indicating the mode of the shallow cumulus droplet distribution (McFarlane and Grabowski, 2007). Figure 4.5 shows the evolutions of the cloud cover and tau. Regarding tau it should be noted that only values of $\tau > 0$ are used in the determination of the average. Our results suggest, in contrary to the findings of Vilà-Guerau de Arellano et al. (2012), that an increase in CO_2 enhances cloud cover and cloud optical thickness. A half-hourly time average (15:30 - 16:00 LT) shows that the cloud cover increases with $\sim 13\%$ and tau with $\sim 5\%$. Due to stomatal closure in the CO2 run, the thermals consist of less moisture compared to the Present run, but the increase in energy and convective velocity as a result of a higher sensible heat flux is sufficient to overcome the drying effect, resulting in more and thicker clouds. This result is in accordance with the study of Vilà-Guerau de Arellano et al. (2014) who found an increased cloud cover above C4 vegetation (stronger and drier thermals) compared to C3 vegetation (weaker thermals transporting less moisture).

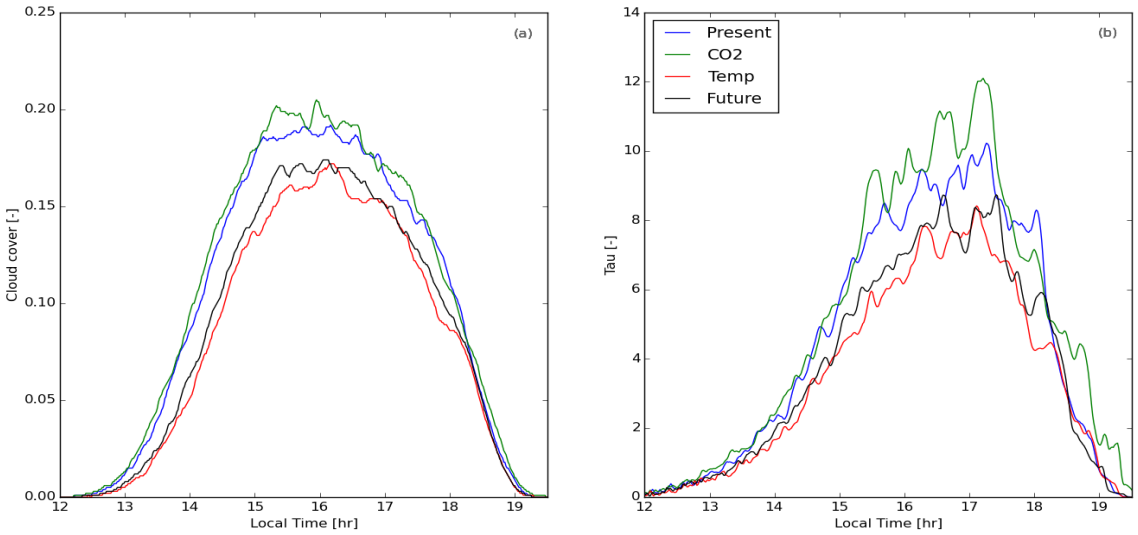

Figure 4.5: Diurnal variation of the cloud cover (a) and tau (b) for all runs, domain averaged. Averaged from 15:00 - 17:00 cloud cover and tau are 0.184 and 8.21 (Present), 0.191 and 9.11 (CO2), 0.157 and 6.37 (Temp) and 0.165 and 6.90 (Future).

In order to provide a deeper explanation for our result, we visualised the tau distribution of the Present run in figure 4.6a, to get a better understanding of the dynamic behaviour and difference in tau. It is found that by far the most clouds are thin ($0 < \tau > 1$), indicating that most clouds do not develop into active clouds. Note that the histogram is normalized, indicating that all values add op to 100%. To identify effects of enhanced CO_2 on the tau distribution, we subtracted the histogram of the Present run (figure 4.6a) from the histogram of the CO2 run, indicating the relative differences in tau between both runs, shown in figure 4.6b. The figure indicates for a certain cloud cover what the relative difference for every range in tau is compared to the Present run. Relative differences with respect to the Present run thus only indicate differences in cloud thickness, not in the amount of clouds. According to figure 4.6b there will be less clouds with a tau ranging from 0 - 15, whereas there will be more clouds with a tau > 15, explaining why the average tau is higher

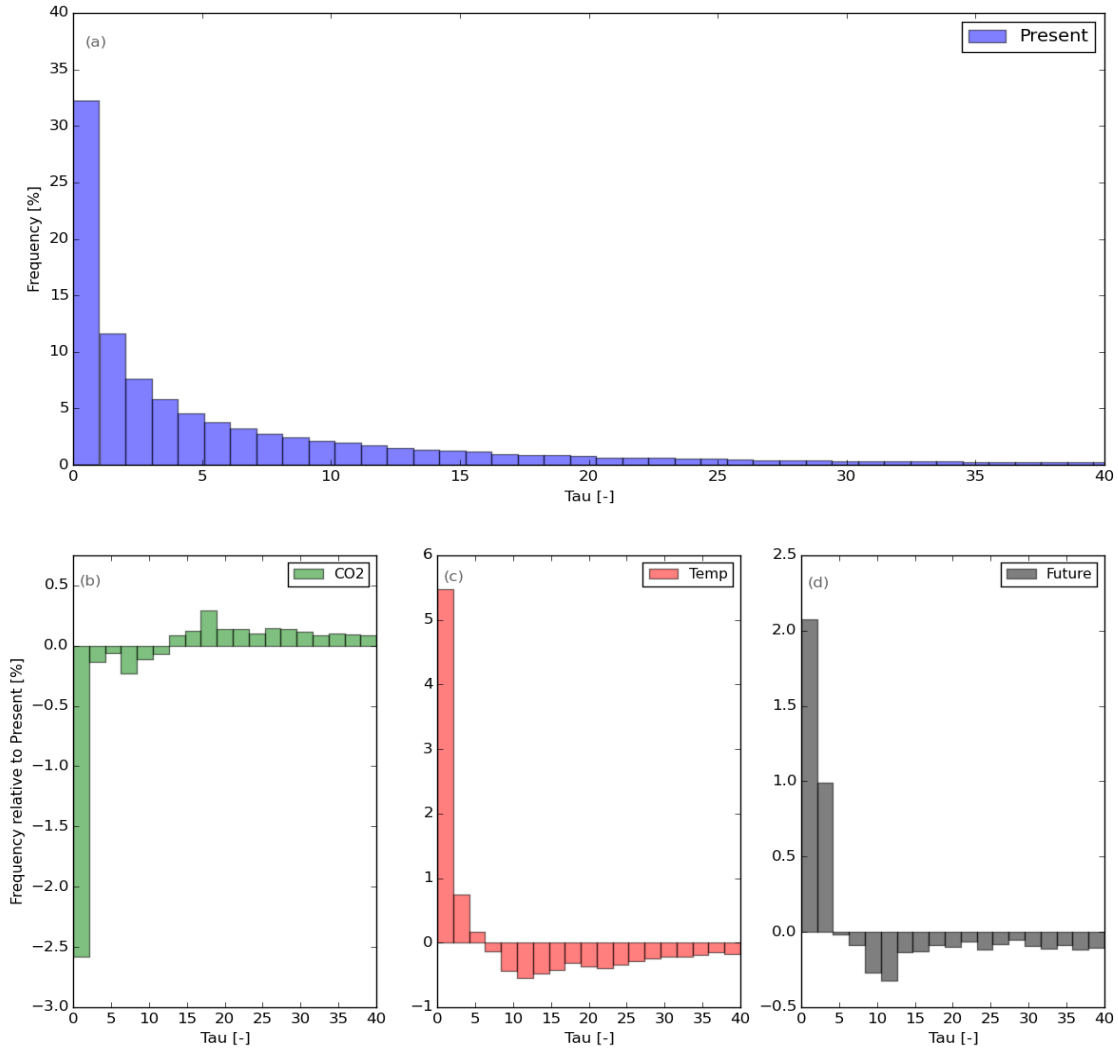

Figure 4.6: Normalized histogram of the distribution of tau for the Present run (a), and the relative difference in tau compared to the Present run, for the CO2 (b), Temp (c) and Future (d) run at 16:00 LT, domain averaged.

in figure 4.5b.

To explain the increase in optical cloud thickness, we connect our analysis to figure 3.3 in section 3. Due to the increase in the sensible heat flux, TKE and thermal strength increase, resulting in more thermals that are able to reach the LCL, indicated by the higher cloud cover compared to the Present run. Furthermore, more thermals are able to reach the LFC as well, where they maintain their development and grow actively into vertically developed cumulus clouds. The largest difference, i.e. 2.5%, is found for $0 < \tau > 1$. This indicates that less thermals are located between the LCL and LFC, i.e. less forced clouds, meaning that more thermals which are able to reach the LCL, also reach the LFC.

Summarizing, a larger amount of thermals that could not develop into a cloud in the Present run, have developed into clouds (forced or active) in the CO2 run and a larger amount of thermals that used to develop into forced clouds in the Present run have developed into active clouds in the CO2 run. This indicates that despite the increase in the CIN (table 4.1), the thermals have

enough energy and velocity to overcome this, reaching higher levels and lower absolute temperatures, favouring condensation. This is corroborated by the increase in CAPE (table 4.1), indicating that more thermals reach the LFC and become positively buoyant.

4.2.2 Effects of warming

The effect of warming is also contrary to the findings of Vilà-Guerau de Arellano et al. (2012) as figure 4.5a shows that warming has an negative effect on cloud formation as the cloud cover decreases with 15%. Figure 4.5b indicates that the optical cloud thickness also decreases, i.e. a 25% decrease for tau. This underlines that energy and thermal strength are the determining factor in cloud formation as those are lower in the Temp run (table 4.1).

There may be more moisture in the boundary layer due to the initial increase of q, but the initial relative humidity was equal to the Present run, maintaining an equal initial vapour pressure deficit as well. Still, based on the increased moisture supply from the surface, a shallower boundary layer leading to less dilution of moisture and on the decreased entrainment flux (less dry air entrainment) it is expected that the relative humidity and vapour pressure deficit would increase for the Temp run. On the other hand, Van Stratum et al. (2014) indicated that due to ventilation of clouds a mass flux transports momentum and energy from the subcloud layer into the cloud layer. As the air that is transported to the cloud layer is relatively moist, this decreases the relative humidity in the subcloud layer. A shallower boundary layer is also characterized by higher absolute temperatures at the CBL_{top} (negative effect on RH), whereas on the other hand less warm air entrainment and a decrease of the sensible heat flux promote cooling of the CBL (positive effect on RH). For a complete overview of all the processes and feedbacks, we refer to Van Stratum et al. (2014). Eventually, table 4.1 shows that both the averaged RH at the surface and at the CBL_{top} do not increase. Therefore, as energy and thermal strength decrease, fewer thermals are able to reach the LCL, indicated by the lower cloud fraction.

If we then focus on figure 4.6b, we observe that warming again has an opposite effect compared to CO_2, resulting in more thinner clouds and less thicker clouds. Due to the decrease in energy and thermal strength, thermals have a smaller probability of reaching the LFC, indicated by the increase in thin clouds in figure 4.6b, resulting in more forced clouds, as they are normally characterized by lower values of tau. So despite that less negative buoyancy has to be overcome, i.e. a lower CIN value, the amount of energy is still not enough to reach the LCL. Also less thermals reach the LFC and become positively buoyant, resulting in a lower CAPE value, shown in table 4.1.

4.2.3 Combined effects of enhanced CO_2 and warming

Since the CO_2 effect was slightly stronger than the temperature effect concerning the surface fluxes (an increase of 3% in the sensible heat flux for the Future run) one would expect that the cloud characteristics of the Future run also would follow the CO2 run more. However, figure 4.5 shows that the Future run is in fact clearly following the Temp run, having a decrease in the cloud cover of 10% and a decrease in tau of 17%. We cannot explain this by means of the energy and thermal strength as those are actually higher compared to the Present run (due to the larger sensible heat flux), indicated in figure 4.3 and table 4.1.

In order to get a better understanding in figure 4.7a the diurnal variation of CBL height, LCL and LFC are plotted for the Present and Future run, whereas in figure 4.7b the diurnal variation in the mutual differences between those levels are plotted, together with the cloud cover on the right y-axis. Figure 4.7a shows that the location of all three levels (CBL height, LCL and LFC) increase in the Future as more vigorous thermals can reach higher levels. Figure 4.7b shows that thermals in the Future run have to travel a larger distance from the CBL height to reach the LCL, i.e. a difference of ~ 24 meters averaged over 15:30 - 16:00 LT (67% increase). This could either be

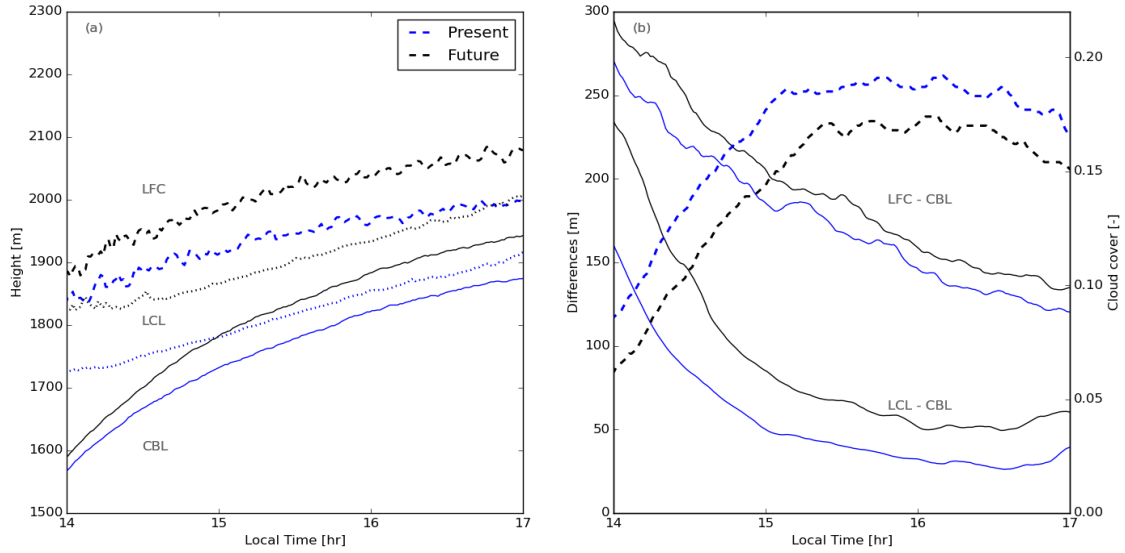

Figure 4.7: Diurnal variation of CBL height, LCL and LFC (a), and moving averages of the mutual differences between CBL height, LCL and LFC on the left y-axis and the cloud cover on the right y-axis (b), for the Present and Future run, domain averaged.

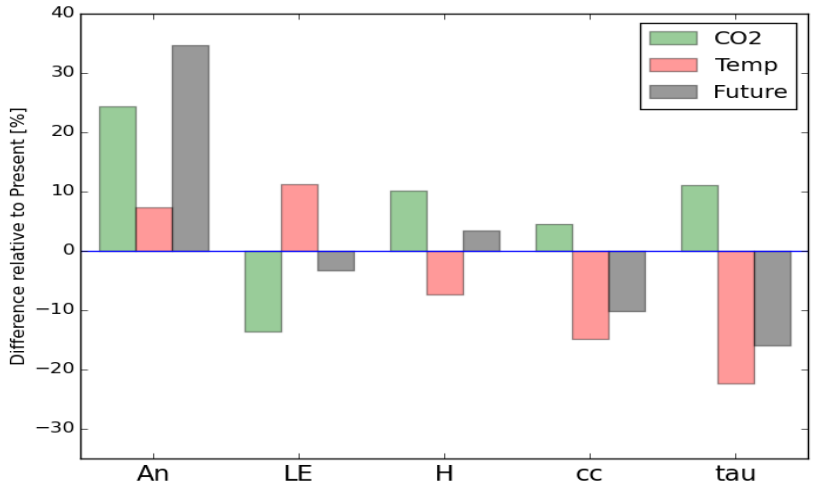

Figure 4.8: Relative differences of A_n, LE, H, cloud cover and tau for the CO2, Temp and Future run compared to the Present run (the blue zero line), averaged over 15:30 - 16:00 LT.

caused by enhanced dry air entrainment, more dilution of moisture as a result of a deeper CBL, by a decrease in the moisture supply from the surface (smaller LE), by warming of the CBL (larger H and more entrainment) or due to a combination of all. Table 4.1 shows that the RH at the CBL height is lower, but only with 1%. Still, a larger distance has to be overcome and the decrease in cloud cover compared to the Present run indicates that the increase in energy is not enough to overcome this extra distance from CBL height to LCL.

Figure 4.7b shows that the difference between the LFC and CBL is also larger, i.e. an increase of $\sim$ 13 meters (9%). However, with a vertical grid spacing of 12 meters, this value is not really significant. Still, focussing on figure 4.6c we observe that, comparable to the Temp run but to a

lesser extent, there are more thinner and more forced clouds. Again linking back to figure 3.3 this indicates that, despite the increase in energy and thermal strength, less thermals are able to reach the LFC as well, corroborated by the lower CAPE value, indicated in table 4.1.

Summarizing section 4.2, concerning the consequences for clouds, the effect of warming is evidently more important than the effect of an enhanced CO_2 concentration, resulting in a lower cloud cover and thinner clouds in a future climate, which is contrary to the findings of Vilà-Guerau de Arellano et al. (2012). In order to visualize all the described effects of enhanced CO_2, warming and the combined forcing, the relative difference of the five most important variables (A_n, LE, H, cloud cover and tau) for the CO2, Temp and Future run compared to the Present run are shown in figure 4.8. More CO_2 and warming both enhanced A_n whereas for the surface fluxes the CO_2 effect was more pronounced, leading to a small increase in the sensible heat flux and a small decrease in the latent heat flux. Concerning the cloud characteristics, warming appeared to be the dominant effect corroborated by the decrease of the cloud cover and cloud thickness (figure 4.8).

5 Discussion

In this study we show that the combined effect of enhanced CO_2 and higher temperatures has an suppressing effect on the formation of surface induced cumulus clouds above the atmospheric boundary layer. This result is comparable to the study of Vilà-Guerau de Arellano et al. (2012), although the impact of the processes, led to the found suppression, is different. The CLASS model in the study of Vilà-Guerau de Arellano et al. (2012) and the LES model in our study give a comparable shift in the partitioning of the surface fluxes as a result of fertilization with CO_2 and warming. Note that Vilà-Guerau de Arellano et al. (2012) increased the CO_2 concentration with 328 ppm, explaining why they observed an even stronger CO_2 effect. Concerning cloud properties, we showed that more CO_2 had a positive effect on cloud formation and temperature a negative effect, which is completely opposite to the results of Vilà-Guerau de Arellano et al. (2012). Effectively, this resulted in an equal outcome as in our study the temperature effects dominated, whereas in the study of Vilà-Guerau de Arellano et al. (2012) the CO_2 effect was stronger.

To explain the differences in the impact of both forcings between the models we link back to the complexity of both models. The CLASS model is based on the mixed-layer equations to obtain the temporal evolution of the boundary layer and surface processes, but lacks spatial variability. Our results suggest that this spatial variability, present in LES, is essential for capturing all the complicated processes and feedbacks that play a role within the development of cumulus clouds. Furthermore, the conclusion of suppressed boundary-layer cloud formation in the study of Vilà-Guerau de Arellano et al. (2012) was based on the difference between the CBL height and the LCL, whereas in our study we indicated that an increase of this distance not necessarily results in fewer clouds.

To improve the mixed-layer formulation within CLASS, Van Stratum et al. (2014) introduced a new developed mass flux parametrization, including all the feedbacks that play a role within the transition from clear to cloud-topped boundary layers. With this extension the model was able to reproduce satisfactory values for the CBL height, θ_v, q_t and cloud-core fraction compared to a LES model (Van Stratum et al., 2014). Therefore, we repeated the study of Vilà-Guerau de Arellano et al. (2012), including the new mass flux parametrization. However, still the CLASS model produced a higher cloud fraction for the run with a higher temperature and a lower cloud fraction for the run with enhanced CO_2. Sikma and Ouwersloot (2015) showed that in the mass flux parametrization of Van Stratum et al. (2014) the active cloud core fraction was overestimated since they did not make a distinction between forced an active clouds, resulting in an overestimation of the mass flux. As we observe a lot of forced clouds in the Temp run and fewer in the CO2 run (figure 4.6), this may explain the different impacts of CO_2 and temperature. Furthermore, the CLASS and the LES model in the study of Van Stratum et al. (2014) had identical prescribed surface fluxes and Van Stratum et al. (2014) already indicated that the importance of including a coupled land surface scheme should be identified by future studies. Based on the results in our study we can conclude that the effect of including this coupled land surface scheme is significant (disregarding the possible effect of an overestimated mass flux) as we find opposite impacts of enhanced CO_2 and temperature. As the LSM is similar in both models (A-g_s) we suggest that the large spatial heterogeneity at the surface, which is not captured by CLASS, is responsible for the discrepancies. Still, more research is needed to provide a full explanation.

As shown by Breshears et al. (1998) and Raich and Schlesinger (1992) soil evaporation and soil respiration play a dominant role within the cloud-atmospheric system as the first has consequences for the water availability, and the latter has an effect on vegetation and climate, especially with higher temperatures. We did not focus on and quantify these effects separately, but they are taken into account by the model. The same holds for the negative feedback loop between transpiration, evaporative cooling and vapour pressure deficit as Sikma et al. (2017) indicated that this negative feedback only played a role at a local scale. Joos et al. (2001) and Qian et al. (2010) indicated that biomass is expected to increase in a future climate, but as we wanted to quantify the effects

of CO_2 and temperature separately, we choose to not consider biomass growth, keeping all the initial plant characteristics and parameters in the A-g_s model constant. For future LES studies a sensitivity analysis could be done by increasing the initial Leaf Area Index (LAI), based on the idea's of Vilà-Guerau de Arellano et al. (2012).

Twomey (1991) indicated that clouds reflect shortwave incoming radiation back to space, whereas it blocks outgoing longwave radiation from the surface. We quantified the differences in net radiation between the four runs, but we did not discussed the different components of the radiation budget (shortwave in and out and longwave in and out). For example, in the CO2 run we observe a decrease of the net radiation with 2%, which could have been caused by the higher amount of reflected incoming shortwave radiation. However, the incoming and outgoing longwave radiation also change as the boundary layer is warmer in the CO2 run. For a full explanation on the radiation budget all the components should be analysed and quantified for every run in order to understand which and why the components change in a future climate.

We are also aware that our conclusions concerning the strength of both forcings are based on an increase of CO_2 with 200 ppm and an increase of temperature with 2 Kelvin, whereas this is only an indication. It is uncertain when these values will be reached and it is also highly uncertain that these increased values for CO_2 and temperature coincide. Climate scenarios indicate that the range in elevated CO_2 and temperature is large (Solomon, 2007), which could have consequences for our results as the CO_2 or temperature effect could be enhanced/decreased. On the other hand, if for example the CO_2 concentration increases more than expected, the temperature will follow as CO_2 and temperature cohere, limiting the consequences for the conclusions of our study.

Finalizing the discussion section, we consider the potential effect of changes on synoptic scales. As our case represented a day in which these synoptics only played a minor role, it would be relevant to study changes in lapse rate (θ_v and q_t), jump of θ_v and q_t at the CBL_{top} and large scale advection. For example, we could study the transition from shallow to deep convection in a future climate, by systematically changing the lapse rate of θ_v and q_t, keeping in mind that the amount of energy and vertical velocity actually was higher in the Future run despite the smaller cloud fraction. A final comment is that the background wind speed was set to zero in our study and the stomatal response was instantaneous. Following the work of Sikma et al. (2017) we could study the cloud-vegetation interaction for different background wind speeds and stomatal responses, but then in a future climate to find out if our conclusions concerning cloud properties change if we introduce wind and a delayed responses of the vegetation as described by Sikma et al. (2017).

6 Conclusion and recommendation

We studied the cloud-vegetation interaction in a future climate by means of an increase in the atmospheric CO_2 concentration and temperature, using the Dutch Atmospheric Large Eddie Simulation (DALES) model coupled to the plant physiological A-g_s model. We selected 23 September 2003, a day that cumulus clouds arose over a well-watered grassland in the Netherlands with a typical convective boundary layer development. We executed four numerical simulations (Present, CO2, Temp and Future) where CO_2 and temperature were separately increased with 200 ppm in the CO2 run and 2 Kelvin in the Temp run, and simultaneously in the Future run. With this approach we were able to disentangle between the effects of both forcings, whereas in the Future run we could also analyse the strength of both forcings relative to each other.

In the CO2 run we show that due to an increase in the external CO_2 concentration photosynthesis rates are enhanced, resulting in an increase of the net assimilation of $\sim 25\%$. Due to the additional CO_2, stomatal aperture is decreased, resulting in an increase of the canopy resistance of $\sim 30\%$. As a result, less moisture enters the atmosphere, thereby decreasing the latent heat flux (LE) with 14% and subsequently increasing the sensible heat flux (H) with 10%, resulting in higher values for TKE, CBL height and convective velocity (stronger thermals). With these more vigorous thermals lower absolute temperatures are reached, resulting in an increase of the cloud cover with $\sim 13\%$ and an increase in the optical cloud thickness τ (tau). This indicates that, concerning cumulus cloud formation, the effect of more energy and stronger thermals dominates over drying effects (more warm and dry air entrainment, moisture dilution due to CBL growth, more heat and less moisture supply from the surface). Since more thermals that have reached the LCL can maintain their development, reach the LFC and grow into active clouds, the distribution of tau shifts to more thick clouds and less thin (forced) clouds.

In the Temp run we observe an increase of the net assimilation with $\sim 7\%$ as under the influence of higher temperatures the photosynthesis rate is enhanced. The stomatal aperture is also temperature dependent as warming decreases the canopy resistance with $\sim 4\%$. The decrease in the canopy resistance together with an increase of the vapour pressure deficit (Clausius-Clapeyron relation) results in an increase of LE with $\sim 11\%$ and a subsequent decrease of H with 7%. This leads to a lower buoyancy flux, CBL height, TKE and convective velocity, resulting in a decrease of the cloud cover with 15% and a decrease in tau with 25%. Again, more energy appeared to be the determining factor in cloud formation as the moistening effects hardly played a role, indicated by the zero increase in averaged relative humidity at the CBL top. As fewer thermals are able to reach the LFC, more forced clouds will arise, indicated by the shift in tau distribution to more thin and less thick clouds.

When both forcings were combined in the Future run, net assimilation increased with 35% and the canopy resistance increased with 25%. Concerning the partitioning of the available energy, the CO_2 effect was somewhat stronger (again based on our indications for CO_2 and temperature increase), indicated by a decrease of LE with $\sim 3\%$ and an increase in H with $\sim 3\%$. This led to stronger thermals and a subsequent increase of the CBL height, LCL and LFC. Remarkably, this resulted not in a larger cloud fraction as cloud cover decreased with 10% and tau decreased with 17%. Also the distribution in tau shifted to more thin and less thick clouds, indicating that concerning clouds, the effect of warming is largely dominating over the enhanced CO_2 effect.

We found that the thermals in the Future run have to travel a larger distance to reach the LCL and LFC, but we could not present a satisfactory reason for this (only an increase of the averaged relative humidity with 1%). Therefore we recommend for further LES studies on this subject, to go into more detail on the processes at top of the boundary layer. We propose to calculate the RH, TKE, CBL height, convective velocity and entrainment only above updrafts and to quantify all involved processes and feedbacks as described by Van Stratum et al. (2014) separately in order to find out which process is dominant. With this approach we should be able to get a better

understanding of why cumulus cloud formation is suppressed in a future climate, although the amount of energy increases.

Acknowledgments

The author is very thankful for the supervision and comments of Martin Sikma, especially for the help with learning how to work with DALES and Python. Also the critical comments of Prof. Dr. Jordi Vilà are highly valued.

References

Ainsworth, E. A. and Long, S. P. (2005). What have we learned from 15 years of free-air co2 enrichment (face)? a meta-analytic review of the responses of photosynthesis, canopy properties and plant production to rising co2. *New Phytologist*, 165(2):351–372.

Ainsworth, E. A. and Rogers, A. (2007). The response of photosynthesis and stomatal conductance to rising [co2]: mechanisms and environmental interactions. *Plant, cell & environment*, 30(3):258–270.

Andrews, T. and Ringer, M. A. (2014). Cloud feedbacks, rapid adjustments, and the forcing–response relationship in a transient co2 reversibility scenario. *Journal of Climate*, 27(4):1799–1818.

Assmann, S. M. (1993). Signal transduction in guard cells. *Annual review of cell biology*, 9(1):345–375.

Betts, A. K. (2004). Understanding hydrometeorology using global models. *Bulletin of the American Meteorological Society*, 85(11):1673–1688.

Bonan, G. B. (1995). Sensitivity of a gcm simulation to inclusion of inland water surfaces. *Journal of Climate*, 8(11):2691–2704.

Boucher, O., Jones, A., and Betts, R. A. (2009). Climate response to the physiological impact of carbon dioxide on plants in the met office unified model hadcm3. *Climate Dynamics*, 32(2-3):237–249.

Breshears, D. D., Nyhan, J. W., Heil, C. E., and Wilcox, B. P. (1998). Effects of woody plants on microclimate in a semiarid woodland: soil temperature and evaporation in canopy and intercanopy patches. *International Journal of Plant Sciences*, 159(6):1010–1017.

Cao, L., Bala, G., Caldeira, K., Nemani, R., and Ban-Weiss, G. (2010). Importance of carbon dioxide physiological forcing to future climate change. *Proceedings of the National Academy of Sciences*, 107(21):9513–9518.

Casso-Torralba, P., Vilà-Guerau de Arellano, J., Bosveld, F., Soler, M. R., Vermeulen, A., Werner, C., and Moors, E. (2008). Diurnal and vertical variability of the sensible heat and carbon dioxide budgets in the atmospheric surface layer. *Journal of Geophysical Research: Atmospheres*, 113(D12).

Chen, F. and Avissar, R. (1994). Impact of land-surface moisture variability on local shallow convective cumulus and precipitation in large-scale models. *Journal of applied Meteorology*, 33(12):1382–1401.

Cheruy, F., Dufresne, J., Hourdin, F., and Ducharne, A. (2014). Role of clouds and land-atmosphere coupling in midlatitude continental summer warm biases and climate change amplification in cmip5 simulations. *Geophysical Research Letters*, 41(18):6493–6500.

Colby Jr, F. P. (1984). Convective inhibition as a predictor of convection during ave-sesame ii. *Monthly Weather Review*, 112(11):2239–2252.

Collins, D. C. and Avissar, R. (1994). An evaluation with the fourier amplitude sensitivity test (fast) of which land-surface parameters are of greatest importance in atmospheric modeling. *Journal of Climate*, 7(5):681–703.

Cramer, W., Bondeau, A., Woodward, F. I., Prentice, I. C., Betts, R. A., Brovkin, V., Cox, P. M., Fisher, V., Foley, J. A., Friend, A. D., et al. (2001). Global response of terrestrial ecosystem structure and function to co2 and climate change: results from six dynamic global vegetation models. *Global change biology*, 7(4):357–373.

Crook, N. A. (1996). Sensitivity of moist convection forced by boundary layer processes to low-level thermodynamic fields. *Monthly Weather Review*, 124(8):1767–1785.

Deardorff, J. W. (1970). Convective velocity and temperature scales for the unstable planetary boundary layer and for rayleigh convection. *Journal of the atmospheric sciences*, 27(8):1211–1213.

Doutriaux-Boucher, M., Webb, M., Gregory, J. M., and Boucher, O. (2009). Carbon dioxide induced stomatal closure increases radiative forcing via a rapid reduction in low cloud. *Geophysical Research Letters*, 36(2).

Gentine, P., Betts, A. K., Lintner, B. R., Findell, K. L., Van Heerwaarden, C. C., and Dandrea, F. (2013). A probabilistic bulk model of coupled mixed layer and convection. part ii: Shallow convection case. *Journal of the Atmospheric Sciences*, 70(6):1557–1576.

Heus, T., Van Heerwaarden, C., Jonker, H., Pier Siebesma, A., Axelsen, S., Dries, K., Geoffroy, O., Moene, A., Pino, D., De Roode, S., et al. (2010). Formulation of the dutch atmospheric large-eddy simulation (dales) and overview of its applications. *Geoscientific Model Development*, 3(2):415–444.

Holtslag, A. and Moeng, C.-H. (1991). Eddy diffusivity and countergradient transport in the convective atmospheric boundary layer. *Journal of the Atmospheric Sciences*, 48(14):1690–1698.

Horn, G., Ouwersloot, H., De Arellano, J. V.-G., and Sikma, M. (2015). Cloud shading effects on characteristic boundary-layer length scales. *Boundary-Layer Meteorology*, 157(2):237–263.

Huang, H.-Y. and Margulis, S. A. (2013). Impact of soil moisture heterogeneity length scale and gradients on daytime coupled land-cloudy boundary layer interactions. *Hydrological Processes*, 27(14):1988–2003.

Jacobs, C. M. and de Bruin, H. A. (1997). Predicting regional transpiration at elevated atmospheric co2: influence of the pbl–vegetation interaction. *Journal of applied meteorology*, 36(12):1663–1675.

Jacobs, C. M. J. (1994). *Direct impact of atmospheric CO2 enrichment on regional transpiration.* Jacobs.

Joos, F., Prentice, I. C., Sitch, S., Meyer, R., Hooss, G., Plattner, G.-K., Gerber, S., and Hasselmann, K. (2001). Global warming feedbacks on terrestrial carbon uptake under the intergovernmental panel on climate change (ipcc) emission scenarios. *Global Biogeochemical Cycles*, 15(4):891–907.

Kruijt, B., Witte, J.-P. M., Jacobs, C. M., and Kroon, T. (2008). Effects of rising atmospheric co 2 on evapotranspiration and soil moisture: a practical approach for the netherlands. *Journal of Hydrology*, 349(3):257–267.

Kuang, Z. and Bretherton, C. S. (2006). A mass-flux scheme view of a high-resolution simulation of a transition from shallow to deep cumulus convection. *Journal of the Atmospheric Sciences*, 63(7):1895–1909.

LeMone, M. A. and Pennell, W. T. (1976). The relationship of trade wind cumulus distribution to subcloud layer fluxes and structure. *Monthly Weather Review*, 104(5):524–539.

Leuning, R. (1995). A critical appraisal of a combined stomatal-photosynthesis model for c3 plants. *Plant, Cell & Environment*, 18(4):339–355.

Lohou, F. and Patton, E. G. (2014). Surface energy balance and buoyancy response to shallow cumulus shading. *Journal of the Atmospheric Sciences*, 71(2):665–682.

Mapes, B. E. (2000). Convective inhibition, subgrid-scale triggering energy, and stratiform instability in a toy tropical wave model. *Journal of the Atmospheric Sciences*, 57(10):1515–1535.

McFarlane, S. A. and Grabowski, W. W. (2007). Optical properties of shallow tropical cumuli derived from arm ground-based remote sensing. *Geophysical research letters*, 34(6).

Monteith, J. (1995). Accommodation between transpiring vegetation and the convective boundary layer. *Journal of Hydrology*, 166(3-4):251–263.

Niu, S., Li, Z., Xia, J., Han, Y., Wu, M., and Wan, S. (2008). Climatic warming changes plant photosynthesis and its temperature dependence in a temperate steppe of northern china. *Environmental and Experimental Botany*, 63(1):91–101.

Ouwersloot, H., Moene, A., Attema, J., and De Arellano, J. V.-G. (2016). Large-eddy simulation comparison of neutral flow over a canopy: Sensitivities to physical and numerical conditions, and similarity to other representations. *Boundary-Layer Meteorology*, pages 1–19.

Pedruzo-Bagazgoitia, X., Ouwersloot, H., Sikma, M., van Heerwaarden, C., Jacobs, C., and Vilà-Guerau de Arellano, J. (2017). Direct and diffuse radiation in the shallow cumulus-vegetation system: enhanced and decreased evapotranspiration regimes. *Journal of Hydrometeorology*, (2017).

Qian, H., Joseph, R., and Zeng, N. (2010). Enhanced terrestrial carbon uptake in the northern high latitudes in the 21st century from the coupled carbon cycle climate model intercomparison project model projections. *Global Change Biology*, 16(2):641–656.

Raich, J. W. and Schlesinger, W. H. (1992). The global carbon dioxide flux in soil respiration and its relationship to vegetation and climate. *Tellus B*, 44(2):81–99.

Ronda, R., De Bruin, H., and Holtslag, A. (2001). Representation of the canopy conductance in modeling the surface energy budget for low vegetation. *Journal of Applied Meteorology*, 40(8):1431–1444.

Seneviratne, S. I., Lüthi, D., Litschi, M., and Schär, C. (2006). Land–atmosphere coupling and climate change in europe. *Nature*, 443(7108):205–209.

Sikma, M. and Ouwersloot, H. (2015). Parameterizations for convective transport in various cloud-topped boundary layers. *Atmospheric Chemistry and Physics*, 15(18):10399–10410.

Sikma, M., Ouwersloot, H., Pedruzo-Bagazgoitia, X., van Heerwaarden, C., and Vilà-Guerau de Arellano, J. (Accepted in 2017). Interactions between active vegetation, atmospheric turbulence and clouds under a wide range of background wind conditions. *Agricultural and Forest Meteorology*, x(x):x.

Soden, B. J. and Held, I. M. (2006). An assessment of climate feedbacks in coupled ocean–atmosphere models. *Journal of Climate*, 19(14):3354–3360.

Solomon, S. (2007). *Climate change 2007-the physical science basis: Working group I contribution to the fourth assessment report of the IPCC*, volume 4. Cambridge University Press.

Stephens, G. L. (1984). The parameterization of radiation for numerical weather prediction and climate models. *Monthly Weather Review*, 112(4):826–867.

Stull, R. B. (1985). A fair-weather cumulus cloud classification scheme for mixed-layer studies. *Journal of Climate and Applied Meteorology*, 24(1):49–56.

Tennekes, H. (1973). A model for the dynamics of the inversion above a convective boundary layer. *Journal of the atmospheric sciences*, 30(4):558–567.

Tiedtke, M., Heckley, W., and Slingo, J. (1988). Tropical forecasting at ecmwf: The influence of physical parametrization on the mean structure of forecasts and analyses. *Quarterly Journal of the Royal Meteorological Society*, 114(481):639–664.

Trenberth, K. E. (2011). Changes in precipitation with climate change. *Climate Research*, 47(1-2):123–138.

Twomey, S. (1991). Aerosols, clouds and radiation. *Atmospheric Environment. Part A. General Topics*, 25(11):2435–2442.

Van Heerwaarden, C. C., Vilà-Guerau de Arellano, J., Moene, A. F., and Holtslag, A. A. (2009). Interactions between dry-air entrainment, surface evaporation and convective boundary-layer development. *Quarterly Journal of the Royal Meteorological Society*, 135(642):1277–1291.

Van Stratum, B. J., Vilá-Guerau de Arellano, J., van Heerwaarden, C. C., and Ouwersloot, H. G. (2014). Subcloud-layer feedbacks driven by the mass flux of shallow cumulus convection over land. *Journal of the Atmospheric Sciences*, 71(3):881–895.

Vilà-Guerau de Arellano, J., Ouwersloot, H. G., Baldocchi, D., and Jacobs, C. M. (2014). Shallow cumulus rooted in photosynthesis. *Geophysical Research Letters*, 41(5):1796–1802.

Vilà-Guerau de Arellano, J., Van Heerwaarden, C. C., and Lelieveld, J. (2012). Modelled suppression of boundary-layer clouds by plants in a co2-rich atmosphere. *Nature geoscience*, 5(10):701–704.

Willmer, C. and Fricker, M. (1996). *Stomata*, volume 2. Springer Science & Business Media.

Wong, S.-C., Cowan, I. R., and Farquhar, G. D. (1985). Leaf conductance in relation to rate of co2 assimilation i. influence of nitrogen nutrition, phosphorus nutrition, photon flux density, and ambient partial pressure of co2 during ontogeny. *Plant physiology*, 78(4):821–825.